blood advances

Dual inhibition of the MEK/ERK and PI3K/AKT pathways prevents pulmonary GVHD suppressing perivenulitis and bronchiolitis

Hiroyuki Muranushi,[1] Takero Shindo,[1] Toyofumi F Chen-Yoshikawa,[2] Akihiko Yoshizawa,[3] Huong Thi Ngo,[1] Fumiaki Gochi,[2] Hiroshi Date,[2] and Akifumi Takaori-Kondo[1]

[1]Department of Hematology/Oncology, [2]Department of Thoracic Surgery, and [3]Department of Diagnostic Pathology, Kyoto University Graduate School of Medicine, Kyoto, Japan

Key Points

- Bronchiolitis and perivascular inflammation with phosphorylation of ERK1/2 and AKT within lymphocytes characterize human pGVHD.

- Dual inhibition of the MEK/ERK and PI3K/AKT pathways prevents bronchiolitis and perivascular inflammation in murine pGVHD.

Patients with pulmonary graft-versus-host disease (pGVHD) have a poor prognosis after allogeneic hematopoietic stem cell transplantation (allo-HSCT). Furthermore, pGVHD pathogenesis is not fully elucidated in humans, and currently available immunosuppressants are inadequately effective. We performed pathologic evaluation of lung specimens from 45 allo-HSCT recipients with pGVHD who underwent lung transplantation. Patient pathology was characterized by bronchiolitis and subpleural perivascular inflammation, with B-cell, monocyte, and T-cell accumulation around bronchioles. Bronchiolitis, perivascular inflammation, and peribronchial macrophage aggregation were also identified in a murine pGVHD model after transplant of bone marrow cells and splenocytes from C57BL/6 to B10.BR mice. Among mitogen-activated protein kinase kinase (MEK) inhibitors, cobimetinib, but not trametinib, improved survival rates. Cobimetinib attenuated bronchiolitis, improved airway resistance and lung compliance in the mice, and suppressed activation of B cells and tumor necrosis factor α production by monocytes in vitro; these features were not suppressed by trametinib or tacrolimus. Furthermore, cobimetinib suppressed activation of phosphatidylinositol 3-kinase/protein kinase B (PI3K/AKT) signaling, resulting in B-cell and monocyte suppression. Dual inhibition of the MEK/extracellular signal-regulated kinase (ERK) and PI3K/AKT pathways using a combination of trametinib and the PI3K inhibitor taselisib strongly suppressed B-cell activation in vitro and improved mouse survival rates compared with vehicle or monotherapy with trametinib or taselisib. Imaging mass cytometry of human pGVHD revealed that T cells around bronchioles were positive for phosphorylated ERK, whereas B cells were positive for phosphorylated AKT. Thus, perivascular inflammation and bronchiolitis mediated by activation of the MEK/ERK and PI3K/AKT pathways are essential for pGVHD and represent a potential novel therapeutic target in humans.

Introduction

Allogeneic hematopoietic stem cell transplantation (allo-HSCT) is a curative treatment for hematologic diseases; however, high levels of treatment-related mortality remain a serious challenge. Graft-versus-host disease (GVHD) is a life-threatening complication, and the use of various immunosuppressants

The full-text version of this article contains a data supplement.

increases rates of relapse of underlying malignancies and treatment-related mortality. Despite advances in the development of molecular targeted reagents[1,2] and cellular therapies,[3] the prognosis for patients with pulmonary GVHD, particularly bronchiolitis obliterans (BO), remains poor.[4,5]

Currently available treatments for BO after allo-HSCT include: triplet therapy with inhaled corticosteroids, azithromycin, and montelukast[6]; extracorporeal photopheresis[7]; and etanercept.[8] However, these treatments are insufficiently effective. Murine models of pulmonary GVHD exhibit donor-derived antibody deposition and germinal center formation,[9] as well as increases in follicular helper T cells and germinal center B cells.[10] Anti–interleukin-21 (IL-21) and anti-CD40L antibodies suppress GVHD by ameliorating antibody deposition. Thus, not only T cells but also B cells, macrophages, neutrophils, and fibroblasts may be involved in BO pathogenesis after allo-HSCT.[11] Nevertheless, immunologic triggers and therapeutic targets in BO have not been elucidated in humans, partly because clinical studies using human lung tissues are lacking.

Human pulmonary GVHD is often accompanied by pleuroparenchymal fibroelastosis (PPFE),[12] an elastic fibrosis in the pleura and subpleural parenchyma, predominantly in the upper lobes, in interstitial pneumonia. We previously reported that PPFE is associated with BO in post-HSCT pulmonary GVHD[13]; however, the pathogenesis of PPFE after HSCT remains unclear.

mitogen-activated protein kinase kinase (MEK) inhibitors are molecular targeted drugs, some of which are now approved by the US Food and Drug Administration for the treatment of malignant melanoma[14,15] and lung cancer.[16] MEK inhibitors also have the potential to control inflammation in chronic obstructive pulmonary disease,[17] and they exhibit antifibrotic effects on murine chronic kidney disease.[18] We have shown that MEK inhibitors suppress human T-cell alloreactivity[19] and intestinal and cutaneous GVHD while preserving graft-versus-tumor effects in mouse models.[20] In addition, phosphorylation of extracellular signal–regulated kinase 1/2 (ERK1/2) in CD4$^+$ T cells may be a predictor of acute GVHD in humans,[21] suggesting that MEK/ERK signaling can be a therapeutic target for human GVHD; however, whether MEK inhibitors are effective in preventing or treating refractory GVHD, such as BO and PPFE, has not been investigated.

Other pathways are also involved in transplantation immunity regulation. The phosphatidylinositol-3 kinase (PI3K)/protein kinase B (AKT)/mammalian target of rapamycin pathway is an intracellular signaling pathway important in cell cycle regulation.[22] PI3K/AKT/mammalian target of rapamycin signaling interacts with the proto-oncogene serine/threonine-protein kinase/MEK/ERK pathway; AKT inhibits the activation of the proto-oncogene serine/threonine-protein kinase.[23] Activation of PI3K/AKT signaling promotes cell cycle progression of T cells[24] and modulates T-cell differentiation.[25] Administration of PI3K inhibitors results in a high incidence of acute GVHD.[26] Hence, these pathways may be important in GVHD onset and warrant further verification.

In the present study, we examined pulmonary GVHD pathology using human histopathologic specimens and assessed the potency of dual inhibition of PI3K/AKT and MEK/ERK signaling in a murine model of pulmonary GVHD.

Materials and methods

Immunohistochemical staining of human lung specimens

Whole lung specimens from patients (N = 45) who underwent lung transplantation at our institution for lung injury after allo-HSCT from 2008 through 2018 were histopathologically evaluated. Written informed consent was obtained from all patients for use of their specimens in this study. Approval for the use of patient specimens was obtained from the Institutional Review Board of Kyoto University (G0469).

Anti-human CD4 (NCL-CD4-1F6; Leica, Tokyo, Japan), CD8 (#M7103; Dako Japan, Kyoto, Japan), CD20 (#M0755; Dako), and CD68 (#N1576; Dako) antibodies were used for immunohistochemical staining. Primary antibodies were applied overnight at 4°C, and specimens were then incubated with biotinylated secondary antibodies for 40 minutes. Avidin-biotin-peroxidase complex (ABC-Elite, Vector Laboratories, Burlingame, CA) at a dilution of 1:100 in bovine serum albumin was then added for 50 minutes.[27] Samples were stained with diaminobenzidine, and nuclei were counterstained with hematoxylin.

Murine bone marrow transplantation

Following previous reports[9,10] with minor modification, 8-week-old B10.BR (H2K^k) mice (Japan SLC, Hamamatsu, Japan) were treated with 120 mg/kg of cyclophosphamide on days −3 and −2, and 7 Gy total body irradiation on day −1, and then infused with 5.0 × 10^6 T cell–depleted bone marrow cells (TCD-BM) and 2.0 × 10^5 T cells, 8.0 × 10^5 splenocytes, or 2.0 × 10^5 T cells plus 4.0 × 10^5 B cells from C57BL/6 (H2K^b) mice (Japan SLC) on day 0. T cells were depleted from bone marrow cells using CD90.2 MicroBeads (Miltenyi Biotec, Bergisch Gladbach, Germany). Cobimetinib (1 mg/kg per day), trametinib (0.1 mg/kg per day), and taselisib (5 mg/kg per day) (all from Selleck Chemicals, Houston, TX) were administered orally and tacrolimus (1 mg/kg per day; Selleck Chemicals) was administered intraperitoneally from day 0 through day 28. Tacrolimus was dissolved in dimethyl sulfoxide (DMSO) and reconstituted in saline, and other reagents were dissolved in DMSO and reconstituted in 200 μL vehicle (methylcellulose/polysorbate buffer).

GVHD severity was evaluated by using a previously reported clinical GVHD scoring system,[28] with minor modifications. Mice were individually scored 3 times per week on a scale from 0 to 2 for six parameters (hunched posture, activity, ruffled fur, alopecia, skin indentation, and diarrhea), and GVHD scores were calculated by summing each score.

On day 42, survival was assessed, and histopathologic evaluation and measurement of respiratory function using flexiVent (emka Technologies, Osaka, Japan) were performed.[29] To exclude the influence of thoracic deformity and cutaneous sclerosis, the chest was opened under anesthesia and respiratory function tests performed while mice were alive. Bone marrow cells and splenocytes from recipients were analyzed by using flow cytometry. Anti-mouse CD4 (EPR19514; Abcam, Cambridge, UK) and B220 (RA3-6B2; Abcam) antibodies were used for immunohistochemical staining, as described for human samples. Quantitative pathologic data were obtained by using QuPath 0.3.0.[30]

Mixed lymphocyte reaction

Based on our previous report,[19] dendritic cells (DCs) were acquired from monocytes collected from healthy human donors that were cultured with granulocyte macrophage-colony stimulating factor (1000 IU/mL; Bayer, Leverkusen, Germany), IL-4 (500 IU/mL; R&D Systems, Minneapolis, MN), IL-1 (10 ng/mL; R&D Systems), tumor necrosis factor α (TNF-α) (10 ng/mL; R&D Systems), IL-6 (15 ng/mL; R&D Systems), and prostaglandin E$_2$ (1 mg/mL; Sigma-Aldrich, St. Louis, MO) for 7 days. Allogeneic peripheral blood mononuclear cells (PBMCs) were labeled with carboxyfluorescein diacetate succinimidyl ester (CFSE) (Thermo Fisher Scientific, Waltham, MA) at 5 μM and cocultured with 25 Gy irradiated DCs for 7 days; cell proliferation was assessed by using flow cytometry as CFSE dilution.

Evaluation of B-cell activation and TNF-α production by monocytes

PBMCs from healthy donors or patients with chronic pulmonary GVHD reconstituted with 200 μL of RPMI 1640 (Nacalai Tesque, Kyoto, Japan) were aliquoted into 96-well plates (1 × 10^6 cells per well) and stimulated with IL-4 (200 IU/mL; R&D Systems) and anti-CD40 antibody (0.3 μg/mL; BioLegend, San Diego, CA) for 24 hours. The frequency of CD20$^+$CD23$^+$CD69$^+$ cells, or the mean fluorescence intensity (MFI) of CD69$^+$ in CD20$^+$CD23$^+$ B cells, was measured by using flow cytometry. Approval for analyzing patients' peripheral blood samples was obtained from the Institutional Review Board of Kyoto University (G0697).

PBMCs reconstituted with 200 μL of RPMI 1640 were aliquoted into 96-well plates (1 × 10^6 cells per well) and stimulated with 1 μg/mL of lipopolysaccharide (Wako Pure Chemical Industries, Osaka, Japan) for 4 hours. Cells were fixed and permeabilized with FIX & PERM A/B buffers (Thermo Fisher Scientific). Intracellular TNF-α and surface staining were analyzed. Intracellular TNF-α was stained with allophycocyanin-conjugated mouse anti–TNF-α (MAb11, BioLegend MAb11), and the frequency of TNF-α–positive cells among CD68$^+$ cells was determined according to flow cytometry.

Flow cytometry

To evaluate phosphorylation of ERK1/2, PBMCs were stimulated with phorbol-12-myristate-13-acetate (PMA) and ionomycin (1 ng/mL:1 mM; Sigma-Aldrich) for 5 minutes in RPMI 1640 supplemented with 10% fetal bovine serum (Thermo Fisher Scientific). Cells were then fixed and permeabilized with FIX & PERM A/B buffers and stained for intracellular phosphorylated ERK1/2 (pERK1/2) and surface antigens. pERK1/2 was stained with rabbit anti-pERK1/2 (Cell Signaling Technology, Danvers, MA) and Alexa 647–conjugated donkey anti-rabbit immunoglobulin G (IgG) (Thermo Fisher Scientific). To evaluate phosphorylation of AKT, PBMCs were stimulated with insulin (Wako Pure Chemical Industries) for 10 minutes. Rabbit anti-phosphorylated AKT (pAKT) antibodies (Cell Signaling Technology) were used. The following antibodies were also used: anti-human CD4 (SK3), CD8 (SK1), CD20 (L27), CD23 (M-L233), CD68 (Y1/82A), and CD69 (FN50); and anti-mouse CD4 (RM4-5), CD19 (1D3), CD62L (MEL-14) (Becton Dickinson, Franklin Lakes, NJ), and CD44 (IM7; BioLegend). Cells were analyzed by using a BD FACSLyric instrument (Becton Dickinson, Franklin Lakes, NJ) with FlowJo software, version 10.4 (Becton Dickinson).

Western blotting

As previously reported,[19] proteins were extracted from PBMCs by using a radioimmunoprecipitation assay buffer (50 mM Tris-HCl, 150 mM NaCl, 0.5% sodium deoxycholate, 0.1% sodium dodecyl sulfate, and 1% NP-40; Thermo Fisher Scientific) supplemented with protease inhibitor (Sigma-Aldrich) and phosphatase inhibitor (Sigma-Aldrich). Proteins were quantified by modified Bradford assay (Bio-Rad, Hercules, CA), resolved by 10% sodium dodecyl sulfate–polyacrylamide gel electrophoresis, transferred to polyvinylidene difluoride membranes (Bio-Rad), and incubated with rabbit anti-human ERK1/2 antibody (Cell Signaling Technology) or mouse anti-human tubulin antibody (Sigma-Aldrich) overnight. Signals were detected on an LAS3000 Imager (Fujifilm, Tokyo, Japan) using horseradish peroxidase–linked anti-mouse IgG or anti-rabbit IgG (Cell Signaling Technology).

Imaging mass cytometry analysis of human lung specimens

Formalin-fixed paraffin-embedded slides of human pulmonary GVHD were dewaxed with xylene, hydrated with ethanol, incubated with antigen retrieval buffer (Agilent, Santa Clara, CA), and blocked with 3% bovine serum albumin. Primary antibodies, including anti-human CD4 (EPR6855), CD8a (RPA-T8), CD20 (H1), CD68 (KP1), pAKT S473 (D9E), and pERK1/2 (D1314.4E) (Fluidigm, South San Francisco, CA), were applied overnight at 4°C. Secondary incubation was with Cell ID intercalator-Iridium (Fluidigm), for 30 minutes at room temperature. Stained tissue samples were interrogated by using a Hyperion Imaging System (Fluidigm), and acquired data were visualized by using the MCD viewer (Fluidigm).

Statistical analysis

Statistical analyses and data presentation were performed by using R software[31] version 4.1.0. Data are expressed as mean ± standard error of the mean (SEM). The log-rank test was used to compare survival between 2 groups, and the two-tailed unpaired t test was used for comparisons between 2 groups of continuous variables. Statistical significance was defined as $P < .05$.

Results

Human pulmonary GVHD is associated with bronchiolitis and perivascular inflammation

First, we evaluated lung specimens from 45 patients with pulmonary GVHD after allo-HSCT who underwent lung transplantation at our hospital from 2008 to 2018. Patient clinical characteristics are summarized in Table 1 and Table 2. Median age was 28 years; the male to female ratio was almost 1:1. Sixty-four percent of the patients received myeloablative conditioning before HSCT. The percentages of patients whose allo-HSCT donor sources were bone marrow, peripheral blood, and cord blood were 60%, 29%, and 11%, respectively. Sixty-four percent could walk <50 m, and 33% had severe respiratory failure requiring mechanical ventilation. Obstructive, restrictive, and mixed ventilatory failure comprised 24%, 31%, and 44% of cases. Seventy-one percent received corticosteroids as treatment for GVHD.

Three characteristic findings were commonly observed on hematoxylin and eosin (H&E)–stained and Elastica van Gieson (EVG)-stained specimens: first, BO (Figure 1A); second, PPFE, with subpleural

Table 1. Characteristics of patients undergoing allo-HSCT

Characteristic	Median (range) or N (%)
Age, y	28 (8-61)
Sex	
Male	24 (53)
Female	21 (47)
Original disease	
AML	17 (38)
ALL	10 (22)
MDS	4 (9)
NHL	6 (13)
AA	3 (7)
Others	5 (11)
HSCT conditioning	
CY/TBI–based MAC	18(40)
BU/CY–based MAC	6 (13)
Other MAC	5 (11)
FLU/MEL–based RIC	3 (7)
FLU/BU–based RIC	4 (9)
Other RIC	3 (7)
Unknown	6 (13)
HSCT donor	
rBM	10 (22)
rPB	13 (29)
uBM	14 (31)
CB	5 (11)
HaploBM	3 (7)
Years from HSCT to development of pulmonary GVHD	
<1 y	20 (44)
1-3 y	13 (29)
>3 y	12 (27)
Years from HSCT to lung transplant	
1-5 y	19 (42)
5-10 y	13 (29)
>10 y	13 (29)

AA, aplastic anemia; AML, acute myeloid leukemia; ALL, acute lymphoid leukemia; BM, bone marrow; BU, busulfan; CB, cord blood; FLU, fludarabine; Haplo, haploidentical; MAC, myeloablative conditioning; MDS, myelodysplastic syndrome; MEL, melphalan; NHL, non-Hodgkin lymphoma; PB, peripheral blood; r, related; RIC, reduced-intensity conditioning; u, unrelated.

proliferation of elastic fibers in the upper lobes of the lung (Figure 1B); and third, peribronchitis in centriacinar areas, macrophage aggregation around bronchi, and cholesterol clefts (Figure 1C). The numbers of patients with these findings are presented in Figure 1E. In total, 90% (42 of 45) of patients had BO, and 70% (31 of 45) showed concomitant BO, PPFE, and peribronchitis. Only 3 cases did not have BO, one of which had organizing pneumonia. Furthermore, 27 of 35 cases with PPFE exhibited lymphocytic infiltration into bronchovascular bundles (Figure 1D), and 21 of 42 cases with BO showed lymphocytic bronchiolitis. These pathologic features were found in multiple locations in the lungs of patients.

Examination of H&E–stained specimens, focusing on bronchiolitis, revealed nearby lymphocyte infiltration (Figure 1F), and immunohistochemical staining detected substantial populations of CD4$^+$ T cells (Figure 1G) and CD8$^+$ T cells (Figure 1H) in peribronchial areas. Interestingly, CD20$^+$ B cells (Figure 1I) and macrophages (Figure 1J) were also abundant, suggesting that B cells and macrophages are associated with the development of pulmonary GVHD.

Collectively, these data indicate that human pulmonary GVHD is commonly characterized by BO, PPFE, and peribronchitis with lymphocyte and monocyte accumulation around bronchioles.

Cobimetinib but not trametinib attenuates murine pulmonary GVHD development

We next performed murine bone marrow transplants that did or did not cause pulmonary GVHD, then verified whether the pathologic findings in mice shared similarities with those in human lung specimens (Figure 1). First, B10.BR mice received TCD-BM only or TCD-BM plus T cells from C57BL/6 mice, after cyclophosphamide (240 mg/kg) administration and 7 Gy total body irradiation (CY/TBI) (Figure 2A-D). Whereas the mice transplanted only with TCD-BM survived until day 42, 80% of those transplanted with TCD-BM + T cells developed diarrhea and died by day 42. Both cobimetinib and trametinib improved survival rates (vehicle 20% vs cobimetinib 70% vs trametinib 80% at day 42; $P = .04$) (Figure 2A). Notably, these mice did not develop bronchiolitis, regardless of treatment type (Figure 2B-C). Hence, T cell–infused mice developed gastrointestinal GVHD, whereas treatment with cobimetinib or trametinib resulted in milder gastrointestinal GVHD and suppressed GVHD scores (Figure 2D).

Next, B10.BR mice received TCD-BM or TCD-BM plus splenocytes (S) from C57BL/6 mice after CY/TBI (Figure 2E-L). Whereas the mice transplanted with TCD-BM only survived until day 42, 69% of those transplanted with TCD-BM + S died by day 42 (Figure 2E); they had mild diarrhea, but their respiratory pathology was fatal, with bronchiolitis (Figure 2F), perivascular inflammation (Figure 2G), and peribronchial macrophage aggregation (Figure 2H) commonly observed in the lungs of TCD-BM + S transplanted mice (Figure 2I). Notably, trametinib and tacrolimus did not improve survival rates, whereas only cobimetinib did (vehicle 31% vs trametinib 7% vs tacrolimus 10% vs cobimetinib 62% at day 42; $P = .01$) (Figure 2E). Cobimetinib suppressed thickening of bronchiole walls and lymphocytic infiltration, while trametinib did not (Figure 2J-K).

Furthermore, mice transplanted with TCD-BM + S exhibited higher airway resistance and lower lung compliance than those transplanted with TCD-BM only. Cobimetinib treatment suppressed the increase in airway resistance (1.65 ± 0.19 cm H_2O.s/mL vs 2.86 ± 0.75 cm H_2O.s/mL; $P < .001$) and the decrease in lung compliance (13.14 ± 0.71 μL/cm H_2O vs 8.99 ± 1.08 μL/cm H_2O; $P = .03$) (Figure 2L-M). Because trametinib-treated mice died or were too weak on day 42, respiratory function tests could not be performed on them.

Immunohistochemical staining of the lungs revealed that cobimetinib and trametinib suppressed CD4$^+$ T-cell infiltration equally relative to vehicle (Figure 2N-O). Of note, cobimetinib inhibited B-cell infiltration more strongly than trametinib (Figure 2P-Q). Cobimetinib also preserved naive T cells in the spleen, while promoting B-cell engraftment in the bone marrow (supplemental Figure 1A-B).

To verify the role of B cells in pulmonary GVHD, B10.BR mice were given TCD-BM with or without B/T cells of C57BL/6 after CY/TBI

Table 2. Characteristics of patients undergoing lung transplantation

Characteristic	Median (range) or N (%)
BMI	15.2 (10.1-25.8)
PCO$_2$	59.5 (34.0-115.0)
Hugh-Jones*	
2-3	2 (4)
4	14 (31)
5	29 (64)
Oxygen	
Nasal/mask	30 (67)
NPPV	9 (20)
Intubated	6 (13)
Pneumothorax	
Yes	29 (64)
No	16 (36)
Respiratory failure	
Obstructive	11 (24)
Restrictive	14 (31)
Mixed	20 (44)
Corticosteroids	
None	13 (29)
2.5-10 mg PSL	16 (36)
12.5-30 mg PSL	16 (36)
Immunosuppressants	
None	34 (76)
Calcineurin inhibitors	9 (20)
MMF	2 (4)
Chronic GVHD in other organs	
None	36 (80)
Skin	5 (9)
Eye	1 (2)
Skin/oral/eye	3 (7)
Concomitant infection	
Aspergillosis	4 (9)
NTM	3 (7)
None	38 (84)
Donors for lung transplantation	
Living	36 (80)
Brain-dead	9 (20)

BMI, body mass index; MMF, mycophenolate mofetil; NPPV, noninvasive positive pressure ventilation; NTM, nontuberculous mycobacteriosis; PCO$_2$, partial pressure of carbon dioxide; PSL, prednisolone.

*Hugh-Jones: 1, able to perform exertion and walk upstairs as well as a healthy person of the same age; 2, able to walk as well as a healthy person of the same age but unable to walk upstairs as well as a healthy person; 3, unable to walk as fast as a healthy person on level ground but able to walk 1 mile at own pace; 4, unable to walk 50 yards without resting; and 5, shortness of breath during conversation, and dressing and undressing, and unable to go out due to shortness of breath.

(Figure 2R). Similarly, cobimetinib (but not trametinib) prolonged survival compared with vehicle-treated controls. Histologic thickening of bronchiole walls with lymphocytic infiltration was observed, which is similar with GVHD after whole splenocyte infusion (supplemental Figure 2).

These results indicate that murine pulmonary GVHD shows pathologic findings of bronchiolitis, perivascular inflammation, and macrophage aggregation around the bronchioles (Figure 2F-H). Notably, these findings are also commonly observed in BO, PPFE, and peribronchitis in humans (Figure 1). In addition, among MEK inhibitors, cobimetinib, but not trametinib, attenuated murine pulmonary GVHD by suppressing B-cell infiltration (Figure 2E,J,P,Q), prompting us to investigate the pharmacologic differences between cobimetinib and trametinib.

Cobimetinib inhibits B-cell and monocyte activation more strongly than trametinib

Next, we tested the differential effects of cobimetinib and trametinib on T cells, B cells, and monocytes in vitro. First, CFSE dilution of human T cells was analyzed in mixed lymphocyte reactions with monocyte-derived DCs and allogeneic PBMCs. Whereas no CFSE dilution of CD4$^+$ and CD8$^+$ T cells was observed in the absence of allogeneic DCs, coculture with allogeneic DCs and DMSO resulted in substantial CFSE dilution (Figure 3A-B). Both cobimetinib and trametinib inhibited CFSE dilution. Given that the clinical serum concentration of cobimetinib was 10 times higher than that of trametinib,[32] these results indicate that cobimetinib inhibits alloreactive T-cell proliferation at an equivalent level to trametinib.

Next, the effects of MEK inhibitors on human B cells were investigated. The MFI of CD69 in CD20$^+$CD23$^+$ cells was evaluated as activation of B cells stimulated with anti-CD40 antibody and IL-4. CD69 MFI was 10 times higher after stimulation than that before stimulation. Interestingly, treatment with cobimetinib led to a greater decrease in CD69 MFI than trametinib (Figure 3C-D).

The suppressive effects of the drugs on human monocytes were also analyzed. After lipopolysaccharide stimulation, 63% of monocytes were positive for TNF-α (Figure 3E). Tacrolimus did not suppress TNF-α production, whereas cobimetinib suppressed TNF-α production more strongly than trametinib (Figure 3E-F).

Thus, cobimetinib suppresses B-cell and monocyte activation more strongly than trametinib.

Cobimetinib, but not trametinib, inhibits PI3K/AKT and MEK/ERK signaling

The differential effects of cobimetinib and trametinib on various kinases were subsequently investigated. Inhibition of ERK1/2 phosphorylation in PMA/ionomycin-stimulated human PBMCs was evaluated by using flow cytometry, which revealed that cobimetinib and trametinib both inhibited ERK1/2 phosphorylation in a dose-dependent manner (Figure 4A-B). Separate western blot analysis of ERK1 and ERK2 phosphorylation revealed that cobimetinib and trametinib also inhibited phosphorylation of both ERK1 and ERK2 in a dose-dependent manner (Figure 4C). These results indicate that both cobimetinib and trametinib inhibit activation of the MEK/ERK pathway equivalently.

Next, the effects of cobimetinib and trametinib on AKT phosphorylation were examined. In T and B cells, AKT is rapidly phosphorylated on stimulation with insulin. Notably, treatment with cobimetinib inhibited phosphorylation of AKT at the T308 position; conversely, trametinib did not inhibit AKT T308 phosphorylation (Figure 4D-E). This difference in phosphorylation was significant in B cells but not in T cells (Figure 4E).
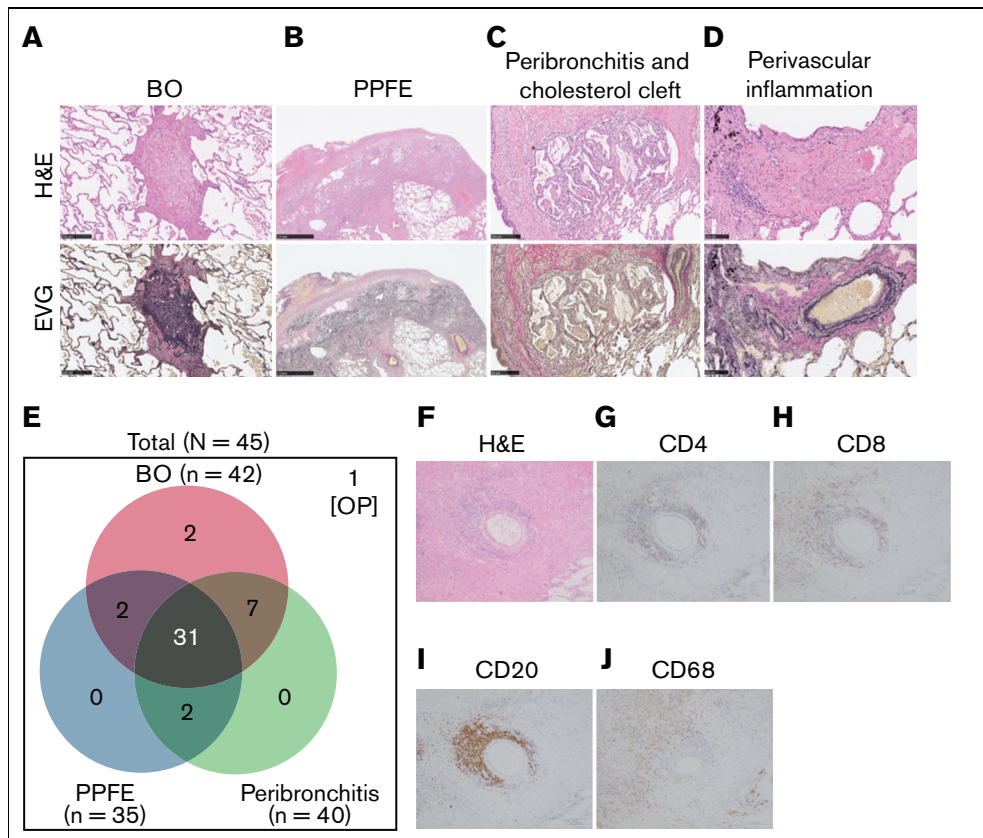
Figure 1. Bronchiolitis, perivascular inflammation, and peribronchitis characterize human pulmonary GVHD. (A-D) Representative images of human pulmonary GVHD. Upper images are H&E stained, and lower figures are EVG stained. (A) BO, (B) PPFE, (C) peribronchitis and cholesterol cleft, and (D) perivascular inflammation. (E) Numbers of patients who had BO, PPFE, peribronchitis, and organizing pneumonia (OP), with overlap among the patients shown. (F-J) Images of specimens stained with H&E (F) or immunohistochemically stained for CD4 (G), CD8 (H), CD20 (I), and CD68 (J) in bronchiolitis.

We then investigated the effects of dual inhibition of the MEK/ERK and PI3K/AKT pathways on human B-cell activation. Frequency of $CD20^+CD23^+CD69^+$ cells was evaluated after stimulation by anti-CD40 antibody and IL-4. Addition of a PI3K inhibitor, taselisib, with trametinib led to an additive decrease in the frequency of $CD23^+CD69^+$ cells (Figure 4F-G).

Next, PBMCs from patients with chronic pulmonary GVHD were analyzed regarding T- and B-cell activation after stimulation with PMA/ionomycin. Their phosphorylation of ERK1/2 within $CD4^+$ T cells was modest compared with healthy donors, but it was substantially inhibited by cobimetinib or trametinib in a dose-dependent manner (supplemental Figure 3A). Meanwhile, stimulation with IL-4 and the anti-CD40 antibody resulted only in few $CD23^+CD69^+$ cells (supplemental Figure 3B), which made it difficult to investigate B-cell suppressive effects of trametinib/cobimetinib.

Dual inhibition of the MEK/ERK and PI3K/AKT pathways suppresses the development of murine pulmonary GVHD

To evaluate the efficacy of combined trametinib and taselisib treatment in murine pulmonary GVHD, TCD-BM and splenocytes from C57BL/6 mice were first transplanted into B10.BR mice (Figure 5). Whereas mice transplanted only with TCD-BM survived until day 42,

77% of mice transplanted with TCD-BM + S died by day 42. Neither trametinib nor taselisib monotherapy improved survival rates; however, cobimetinib monotherapy and combination therapy with trametinib and taselisib increased mouse survival (vehicle 23% vs trametinib 0% vs taselisib 18% vs cobimetinib 64% vs combination 58%, at day 42) (Figure 5A). Histopathologic analysis showed that cobimetinib monotherapy or combination therapy with taselisib plus trametinib suppressed lymphocytic infiltration into peribronchial and perivascular areas, whereas taselisib did not (Figure 5B-C). Moreover, cobimetinib monotherapy or combination therapy with taselisib and trametinib, but not taselisib monotherapy, suppressed infiltration of $CD4^+$ T cells and B cells around the bronchioles (Figure 5D-E). Mice treated with trametinib died before day 42 and could not be histologically evaluated. Thus, dual inhibition of the MEK/ERK and PI3K/AKT pathways can suppress pulmonary GVHD in vivo.

B and T cells in human pulmonary GVHD are positive for pERK and phosphorylated AKT

Finally, imaging mass cytometry of human pulmonary GVHD specimens was conducted by using the Hyperion Imaging System. Among all the pulmonary GVHD cases collected, we specifically focused on 7 cases of lymphocytic bronchiolitis and BO with rich lymphocyte infiltration. Five patients received corticosteroids, and 2 did not take any immunosuppressants. One patient had both pulmonary and cutaneous GVHD, and 6 had pulmonary GVHD alone. Representative
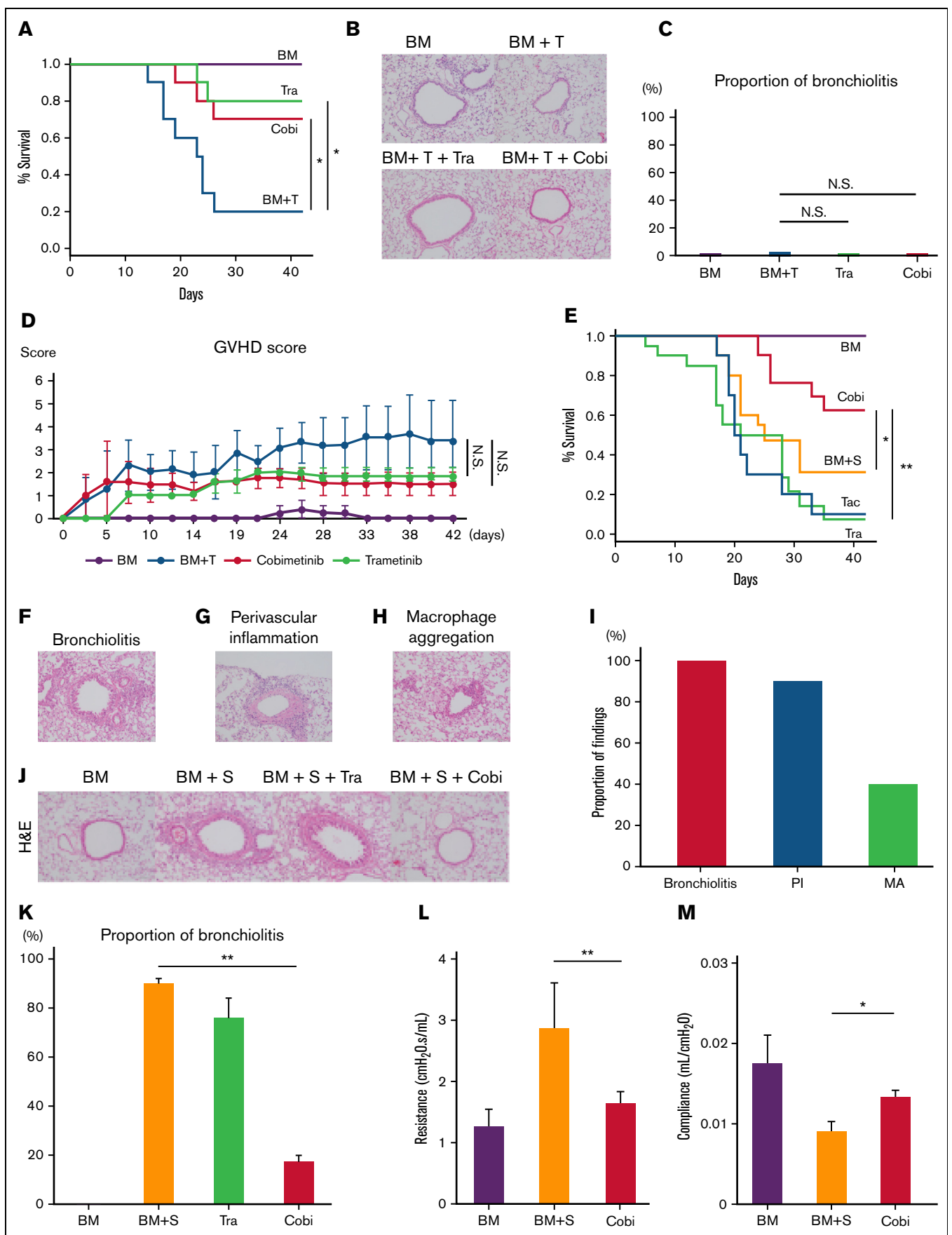
Figure 2. Cobimetinib suppresses murine pulmonary GVHD, whereas trametinib does not. (A-D) B10.BR mice were treated with CY/TBI and transplanted with bone marrow cells (BM) only or BM plus T cells (BM + T) from C57BL/6 mice. (A) Survival curves of mice (n = 10 per group) transplanted with BM or BM + T and treated with
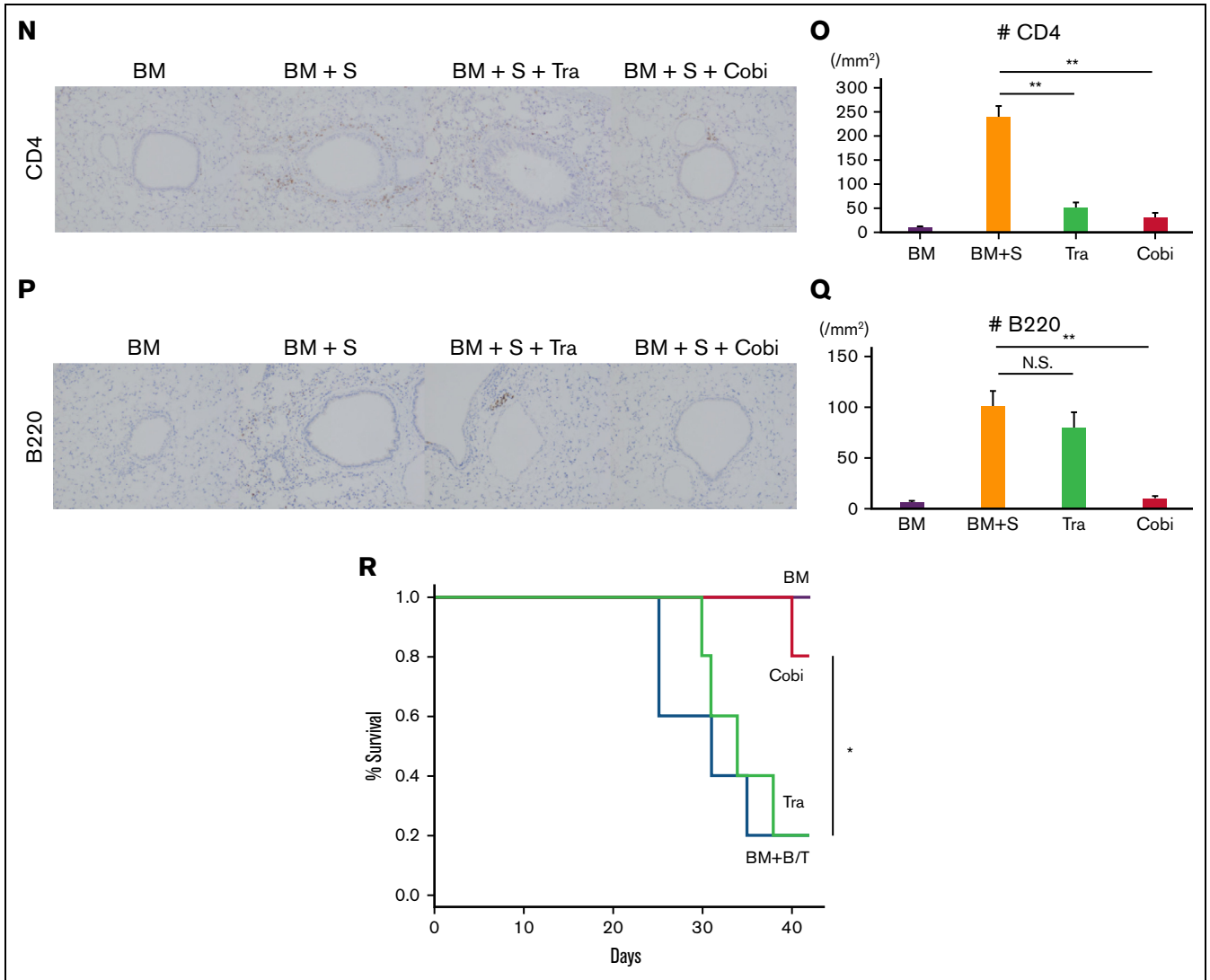
Figure 2 (continued) trametinib or cobimetinib. Transplantations were performed twice, independently. (B) H&E–stained specimens of bronchioles from mice transplanted with BM or BM + T and treated with trametinib or cobimetinib. Proportions of bronchiolitis among all bronchioles (C) and clinical GVHD scores (D) of the mice. (E-Q) B10.BR mice were treated with CY/TBI and transplanted with BM only or BM plus splenocytes from C57BL/6 mice. (E) Survival curves of mice transplanted with BM or BM + S and treated with trametinib, cobimetinib, or tacrolimus. Tacrolimus-treated group, n = 10 mice; other groups, n = 20 mice. Transplantations were performed 4 times independently. (F-H) Pathologic images of H&E–stained specimens from mice transplanted with BM + S: bronchiolitis (F), perivascular inflammation (G), and macrophage aggregation (H). (I) Proportions of mice with bronchiolitis, perivascular inflammation (PI), and macrophage aggregation (MA) among 10 mice given BM + S. (J) Representative pathologic images of H&E–stained tissues around bronchioles. (K) Proportions of bronchiolitis in all mouse bronchioles (n = 5 mice per group). Bars, mean values; error ranges, standard error of the mean (SEM). (L) Airway resistance of the mice is shown. Bars, mean values; error range, SEM. (M) Bar graphs of lung compliance data are shown. Bars, mean; error range, SEM. (N-Q) Immunohistochemically stained murine lung specimens. Representative images of CD4 staining (N) and numbers of CD4^{+} cells in peribronchial areas (O) (n = 5 per group). Representative images of B220 staining (P) and numbers of B220^{+} cells in peribronchial areas (Q) (n = 5 per group). (R) B10.BR mice were treated with CY/TBI and transplanted with BM only, or BM with B and T cells from C57BL/6 mice. Survival curves of mice (n = 10 per group) transplanted with BM or BM + B/T cells and treated with trametinib or cobimetinib. Transplantations were performed twice independently. The log-rank test was used to compare survival rates between the 2 groups, and the two-tailed unpaired t test was used for comparisons between 2 groups of continuous variables. *$P < .05$, **$P < .01$. Cobi, cobimetinib; N.S., not significant; Tra, trametinib.

images from 2 patients with substantial lymphocytic infiltration are presented in Figure 6A-H; patient #1 had BO, and patient #2 had lymphocytic bronchiolitis. Images of specimens from patient #1 stained with H&E and EVG revealed BO and perivascular inflammation (Figure 6A). Furthermore, imaging mass cytometry revealed that CD4^{+}, CD8^{+}, and CD68^{+} cells were diffusely infiltrated around the bronchioles, whereas CD20^{+} cells formed clusters around the bronchioles and blood vessels (Figure 6B). Most of the CD20^{+} cells were
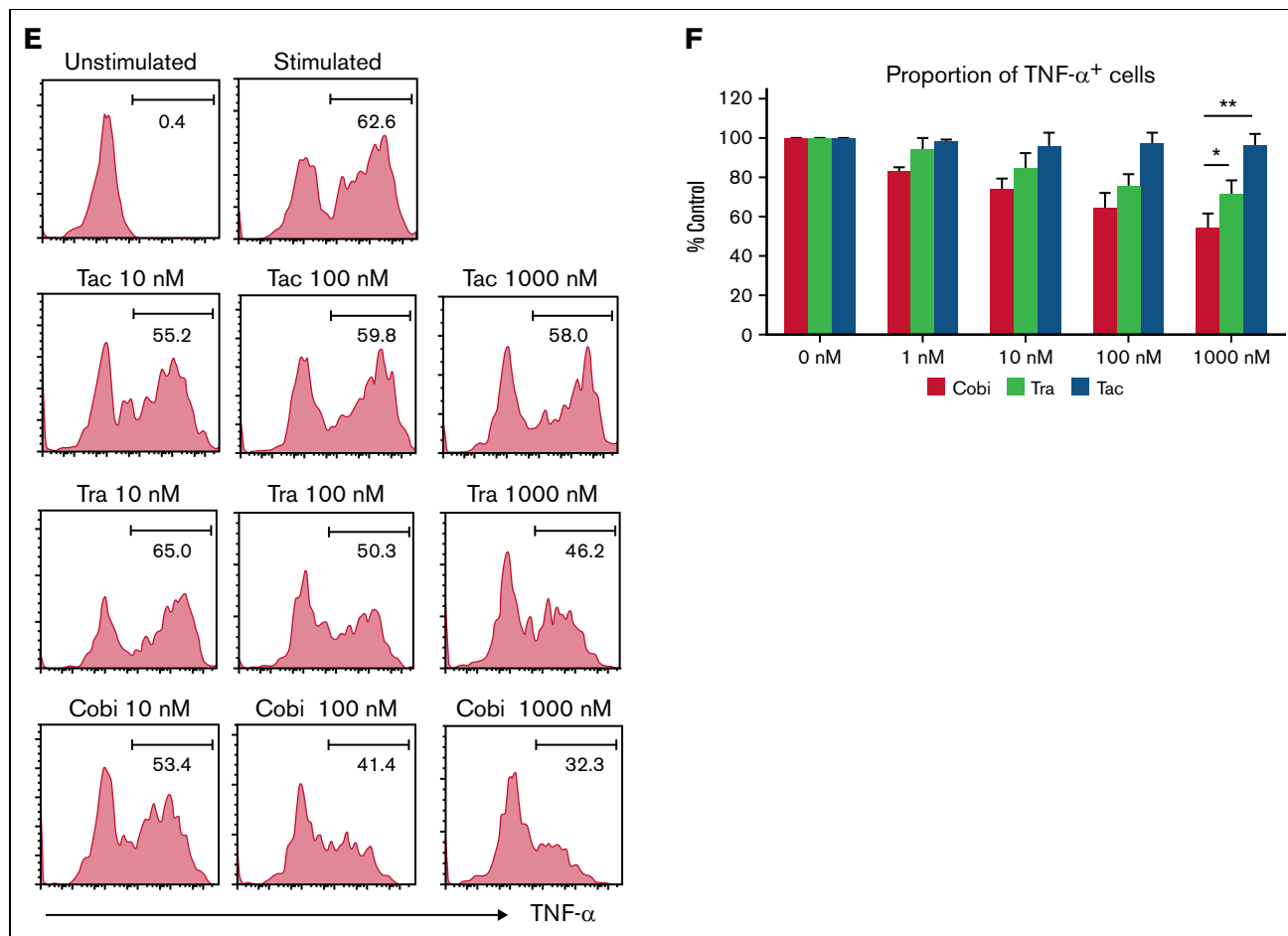
positive for phosphorylated AKT, whereas pERK was partially positive in CD4^{+} and CD8^{+} cells (Figure 6C-D).

Images of specimens from patient #2 stained with H&E and EVG revealed lymphocytic infiltration around bronchioles (Figure 6E). Most CD20^{+}, CD4^{+}, and CD8^{+} cells were positive for phosphorylated AKT, whereas pERK was positive only in some CD4^{+} and CD8^{+} cells (Figure 6F-H). Summative data on pERK in CD4^{+} and
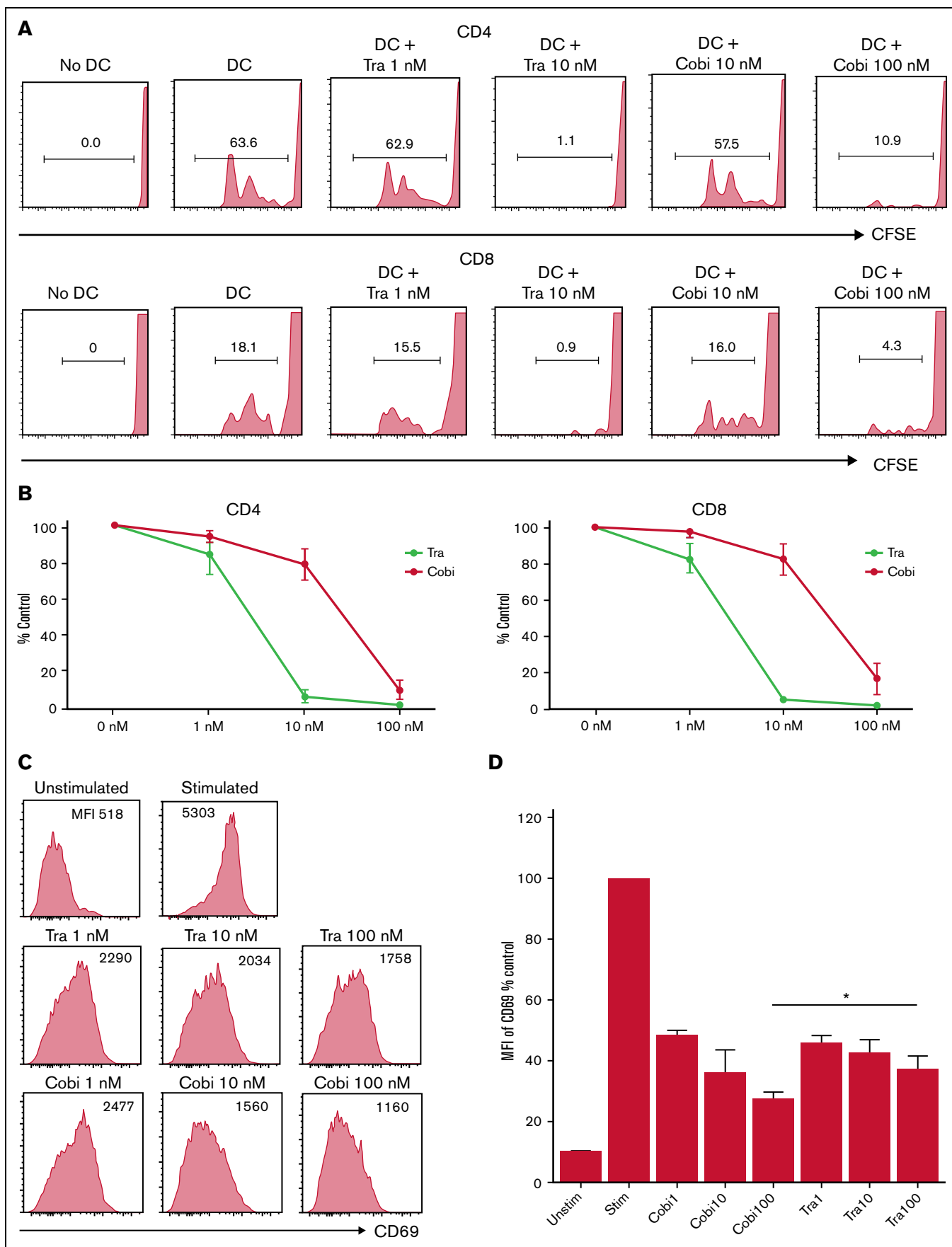
Figure 3. Cobimetinib inhibits activation of B cells and TNF-α production by monocytes more strongly than trametinib. (A-B) PBMCs were stimulated with allogeneic DCs and CFSE dilution evaluated in CD4^{+} and CD8^{+} T cells: representative data (A) and aggregate data (B). The line graph plots the mean value; error range,

E

Unstimulated	Stimulated
0.4	62.6

Tac 10 nM	Tac 100 nM	Tac 1000 nM
55.2	59.8	58.0

Tra 10 nM	Tra 100 nM	Tra 1000 nM
65.0	50.3	46.2

Cobi 10 nM	Cobi 100 nM	Cobi 1000 nM
53.4	41.4	32.3

TNF-α

F Proportion of TNF-α$^+$ cells

Cobi Tra Tac

Figure 3 (continued) standard error of the mean (SEM). (C-D) PBMCs were exposed to trametinib and cobimetinib, and the MFI values of CD69$^+$ cells among CD20$^+$CD23$^+$ cells after stimulation with anti-CD40 antibody and IL-4 were evaluated: representative data (C) and aggregate data (D). The bar graph plots the mean value; error range, SEM. (E-F) PBMCs were stimulated with lipopolysaccharide, and frequencies of TNF-α$^+$ cells among monocytes were evaluated: representative data (E) and aggregate data (F). The bar graph plots the median value; error range, SEM. All experiments were performed 4 times, independently. A two-tailed unpaired t test was used for comparisons between 2 groups of continuous variables. *$P < .05$, **$P < .01$. Cobi, cobimetinib; Tra, trametinib.

CD8$^+$ cells and phosphorylated AKT in CD20$^+$ cells from the 7 patients are presented in Figure 6I. Collectively, these results provide a rationale for targeting the MEK/ERK and PI3K/AKT pathways to suppress pulmonary GVHD in humans.

Discussion

In the present study, we examined the pathology of human pulmonary GVHD specimens and the potency of MEK inhibitors in murine pulmonary GVHD models. We found that bronchiolitis and perivascular inflammation were associated with pulmonary GVHD and that dual inhibition of the MEK/ERK and PI3K/AKT pathways prevented bronchiolitis and perivascular inflammation in a murine pulmonary GVHD model. Based on our results, we propose that BO, PPFE, and peribronchitis be included in the criteria for pathologic diagnosis of pulmonary GVHD, which has potential for translation to develop a novel treatment strategy.

The involvement of B cells and macrophages in chronic GVHD pathogenesis has been reported previously.[33,34] Regarding drugs that inhibit B-cell activation, ibrutinib, an irreversible inhibitor of

Bruton's tyrosine kinase and IL-2–inducible tyrosine kinase, has been approved by the US Food and Drug Administration for the treatment of chronic GVHD,[2] and spleen tyrosine kinase inhibitors can attenuate murine GVHD.[35,36] Of drugs that inhibit macrophage activation, pirfenidone ameliorates murine pulmonary GVHD.[37] However, these drugs inhibit only B cells or macrophages and cannot simultaneously inhibit the activation of various cells involved in pulmonary GVHD. Conversely, MEK inhibitors can simultaneously suppress the activation of cells, including T cells, B cells, and monocytes, because the MEK/ERK pathway is involved in activation of all these cell types, as shown in our investigations.

PPFE is believed to be triggered by excessive interstitial inflammation.[38] In addition, PPFE after allo-HSCT and alveolar fibroelastosis in restrictive allograft syndrome after lung transplantation have common pathologic characteristics,[12,39] suggesting that PPFE is associated with an alloimmune response; however, the details of PPFE pathogenesis remain unclear. We assume that insufficient circulation may cause PPFE in human lung specimens because we frequently observed subpleural perivascular inflammation, indicating that subpleural inflammation likely causes ischemia, leading to
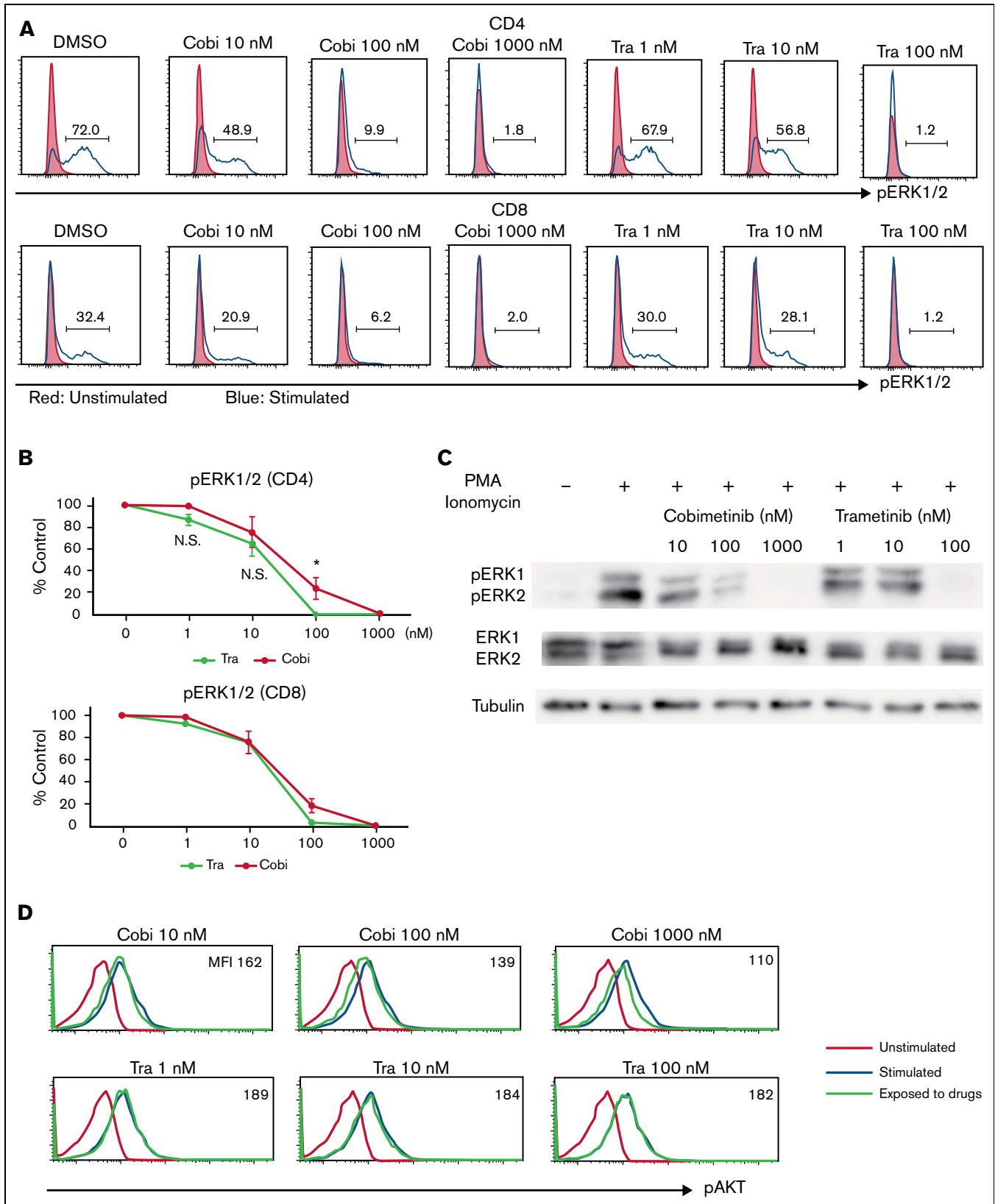
Figure 4. Cobimetinib, but not trametinib, inhibits both PI3K/AKT and MEK/ERK signaling. (A-B) PBMCs were stimulated with PMA and ionomycin, and phosphorylation of ERK1/2 within CD4$^+$ and CD8$^+$ T cells was evaluated by flow cytometry: representative data (A) and aggregate data (B). The line graph plots the mean value; error range, standard error of the mean (SEM). (C) PBMCs were stimulated with PMA and ionomycin, and total ERK1/2 and pERK1/2 were evaluated by western blotting.
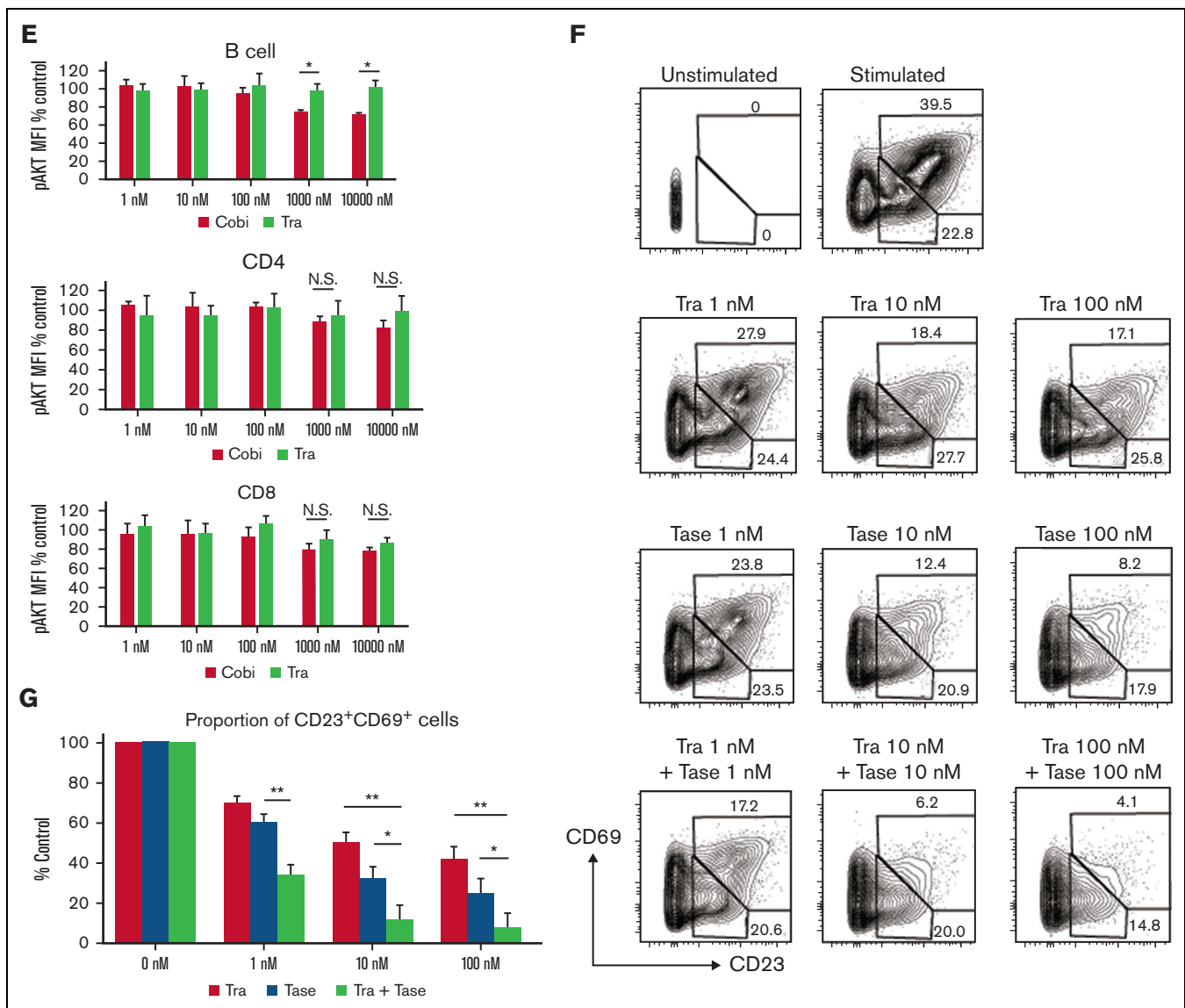
Figure 4 (continued) (D-E) B or T cells were stimulated with insulin, and phosphorylation of AKT was evaluated by flow cytometry: representative data (D) and aggregate data (E). Bars, MFI values with SEM. (F-G) PBMCs were exposed to trametinib, taselisib, or both drugs, and frequencies of CD20⁺CD23⁺CD69⁺ cells after stimulation with anti-CD40 antibody and IL-4 were evaluated: representative data (F) and aggregate data (G). Bars, mean values; error range, SEM. All experiments were performed 4 times, independently. A two-tailed unpaired *t* test was used for comparisons between 2 groups of continuous variables. *$P < .05$, **$P < .01$. Cobi, cobimetinib; N.S., not significant; pAKT, phosphorylated AKT; pERK, phosphorylated ERK; Tase, taselisib; Tra, trametinib.

fibrosis. We did not observe PPFE in the murine pulmonary GVHD model, possibly because the development of fibrosis is a lengthy process, and our experiments were of relatively limited duration; however, perivascular inflammation of both human and murine pulmonary GVHD specimens was observed. Because cobimetinib suppressed the development of these features in the mouse model, we consider it likely that cobimetinib can suppress the development of PPFE in humans. A previous report showed that histologically, pulmonary GVHD is characterized by intrabronchiolar T cells, apoptosis, and perivenulitis.[40] Because T-cell infiltration around bronchioles causes BO, apoptosis is associated with macrophage aggregation, and perivenulitis is associated with PPFE, our results are consistent with those presented in this previous report.

The MEK/ERK and PI3K/AKT pathways are involved in lymphocyte and monocyte proliferation and differentiation.[19,41,42] PI3K/AKT signaling is conversely activated by MEK inhibitors in murine models,[43] consistent with our results showing that simultaneous inhibition of the MEK/ERK and PI3K/AKT pathways more potently suppressed human lymphocyte and monocyte activation. The MEK/ERK and PI3K/AKT pathways are also involved in intestinal epithelial cell and skin epidermal cell proliferation, and complete inhibition of both pathways may lead to increased adverse events such as skin rashes and diarrhea.[44] Combination of trametinib and taselisib is an attractive option, but there are non-negligible risks of unknown side effects due to drug interactions. The side effects of cobimetinib include potential hepatic or renal impairment but are generally
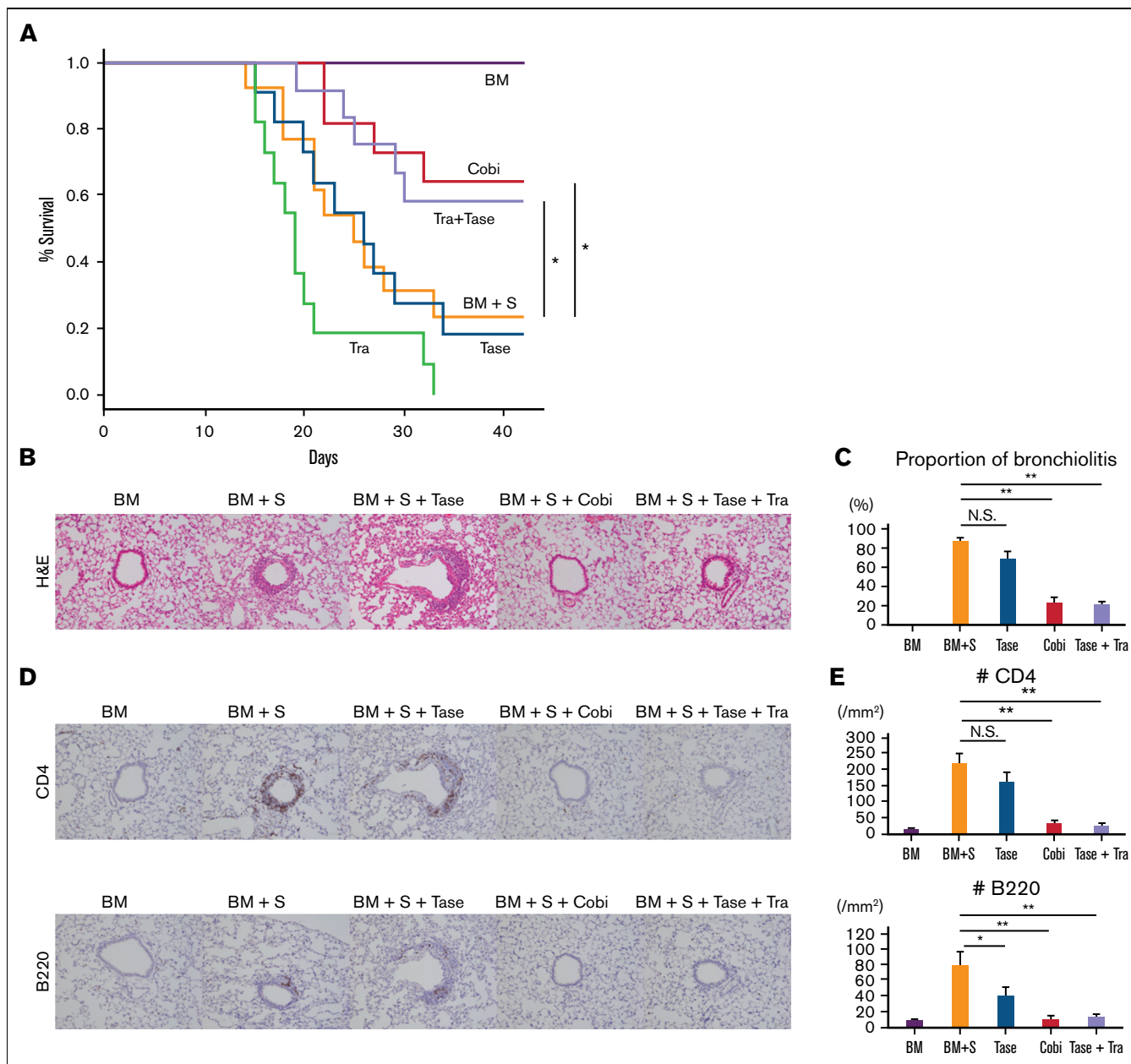
Figure 5. Treatment with a combination of trametinib and taselisib inhibits the development of pulmonary GVHD in mice. B10.BR mice were given CY/TBI and were transplanted with bone marrow cells (BM) only, or bone marrow cells plus splenocytes (BM + S) from C57BL/6 mice. Trametinib, taselisib, cobimetinib, and trametinib plus taselisib were administered. (A) Survival curves of recipient mice are shown. Vehicle or combination therapies, n = 12 per group; others, n = 11 per group. Transplantations were performed twice, independently. (B) Pathologic images around bronchioles of lung specimens stained with H&E. (C) The proportions of bronchiolitis in all bronchioles in mice receiving BM/BM + S and treated with taselisib, cobimetinib, or taselisib + trametinib (n = 5 per group). Bars, mean values; error range, standard error of the mean. (D) Immunohistochemically stained images of murine bronchioles. Upper, CD4; lower, B220. (E) Numbers of CD4+ and B220+ cells in the peribronchial areas (n = 5 per group). Bars, mean values; error range, standard error of the mean. The log-rank test was used to compare survival between 2 groups, and a two-tailed unpaired t test was used for comparisons between 2 groups of continuous variables. *$P < .05$, **$P < .01$, Cobi, cobimetinib; N.S., not significant; Tase, taselisib; Tra, trametinib.

tolerable.[45] Trametinib has high selectivity for MEK and does not inhibit other kinases.[46] Cobimetinib inhibits phosphorylation of AKT T308 in addition to MEK/ERK, which raises translational potential for suppression of pulmonary GVHD without increased adverse events.

The present study found that MEK inhibitors promoted B-cell engraftment in the bone marrow and suppressed B-cell infiltration in the lung in a murine lung GVHD model. We previously showed that MEK inhibitors ameliorate murine intestinal/cutaneous GVHD while preserving graft-versus-tumor effects[20] as well as promoting immune reconstitution in a xenogeneic GVHD model.[47] MEK inhibitors may also be promising in terms of separating GVHD from antitumor/anti-infective immunity.

118   MURANUSHI et al
10 JANUARY 2023 • VOLUME 7, NUMBER 1   blood advances
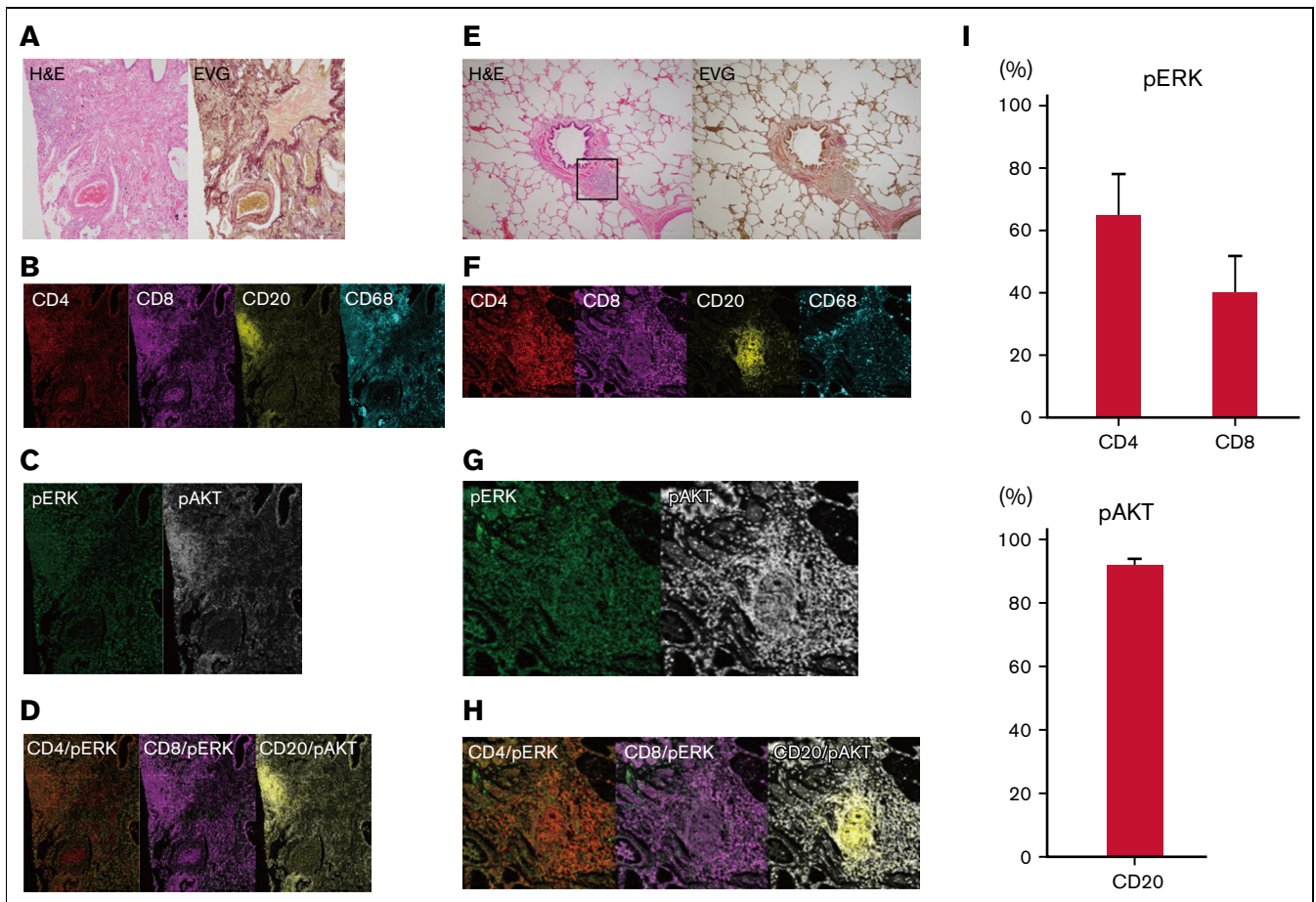
Figure 6. T cells around bronchioles in human pulmonary GVHD are positive for pERK and B cells are positive for phosphorylated AKT (pAKT). Representative images of tissue samples from human patients with pulmonary GVHD. (A) Images of specimens from patient #1 stained with H&E or EVG. BO (upper right) and perivenulitis (lower left) were present. (B-D) Images of samples from patient #1 captured by imaging mass cytometry: (B) CD4, CD8, CD20, and CD68; (C) pERK and pAKT; (D) merged images of CD4/pERK, CD8/pERK, and CD20/pAKT. (E) Images of specimens from patient #2 stained with H&E or EVG. The area enclosed by the square was analyzed by imaging mass cytometry. (F-H) Images from patient #2 captured by imaging mass cytometry: (F) CD4, CD8, CD20, and CD68; (G) pERK and pAKT; (H) merged images of CD4/pERK, CD8/pERK, and CD20/pAKT. (I) Proportions of pERK-positive CD4$^+$ and CD8$^+$ cells, and pAKT-positive CD20$^+$ cells (n = 7). pAKT, phosphorylated AKT; pERK, phosphorylated ERK.

The present study has some limitations. First, we could not confirm B-cell activation in the patients' PBMCs (supplemental Figure 3). This result may be attributed to the fact that the patients took several immunosuppressants, including calcineurin inhibitors and corticosteroids, for several months. B-cell activation status may be different in peripheral blood and the lungs, which should be further investigated. Second, it is unknown what types of toxicities are observed when MEK and PI3K inhibitors are administered to human GVHD patients. If skin rash or diarrhea worsens after administration of MEK and PI3K inhibitors, it may be difficult to differentiate whether those are worsening of GVHD or toxicities of the drugs. Third, the time course of activation of the MEK/ERK and PI3K/AKT pathways in human GVHD has not been clarified. The best timing of inhibiting MEK/ERK and PI3K/AKT pathways should be explored.

In conclusion, human pulmonary GVHD is associated with bronchiolitis and circulatory failure due to perivascular inflammation, and cells other than T cells, such as B cells and monocytes, play important roles in pulmonary GVHD pathogenesis. Cobimetinib suppresses the onset of bronchiolitis and perivascular inflammation in a murine model of pulmonary GVHD by inhibiting the activation of T cells, B cells, and monocytes. These results suggest that cobimetinib has potential for use as a prophylactic agent against human pulmonary GVHD. Clinical application of cobimetinib for GVHD prophylaxis is warranted.

Authorship

Contribution: H.M. performed the experiments, collected and analyzed the data, and wrote the manuscript; T.S. conceived the primary hypothesis, designed and organized the study, and wrote the manuscript; T.F.C.-Y. performed human lung transplantation and helped collect the data on human lung specimens; A.Y. evaluated murine and human pathologic specimens and edited the manuscript; H.T.N. helped with murine bone marrow transplantation; F.G. helped with murine respiratory function tests; H.D. performed human lung transplantation and supervised the project; A.T.-K. supervised the project; and all authors confirmed the final version of the manuscript and approved it for publication.

Conflict-of-interest disclosure: T.S. received research funds from Bristol Myers Squibb. A.Y. received research funds from AcuSolutions. The remaining authors declare no competing financial interests.

ORCID profiles: H.M., 0000-0003-3195-2322; T.S., 0000-0002-2085-6151; F.G., 0000-0001-7193-0609; H.D., 0000-0001-7262-6000; A.T.-K., 0000-0001-7678-4284.

Correspondence: Takero Shindo, Department of Hematology/Oncology, Kyoto University Graduate School of Medicine, Kyoto, Japan, 54 Kawahara-cho, Shogo-in, Sakyo-ku, Kyoto 606-8507, Japan; email: takeros@kuhp.kyoto-u.ac.jp.

References

1. Zeiser R, von Bubnoff N, Butler J, et al; REACH2 Trial Group. Ruxolitinib for glucocorticoid-refractory acute graft-versus-host disease. *N Engl J Med*. 2020;382(19):1800-1810.

2. Miklos D, Cutler CS, Arora M, et al. Ibrutinib for chronic graft-versus-host disease after failure of prior therapy. *Blood*. 2017;130(21):2243-2250.

3. Le Blanc K, Frassoni F, Ball L, et al; Developmental Committee of the European Group for Blood and Marrow Transplantation. Mesenchymal stem cells for treatment of steroid-resistant, severe, acute graft-versus-host disease: a phase II study. *Lancet*. 2008;371(9624):1579-1586.

4. Palmer J, Williams K, Inamoto Y, et al. Pulmonary symptoms measured by the National Institutes of Health lung score predict overall survival, nonrelapse mortality, and patient-reported outcomes in chronic graft-versus-host disease. *Biol Blood Marrow Transplant*. 2014;20(3):337-344.

5. Nakasone H, Kanda J, Yano S, et al; GVHD Working Group of the Japan Society for Hematopoietic Cell Transplantation. A case-control study of bronchiolitis obliterans syndrome following allogeneic hematopoietic stem cell transplantation. *Transpl Int*. 2013;26(6):631-639.

6. Williams KM, Cheng GS, Pusic I, et al. Fluticasone, azithromycin, and montelukast treatment for new-onset bronchiolitis obliterans syndrome after hematopoietic cell transplantation. *Biol Blood Marrow Transplant*. 2016;22(4):710-716.

7. Del Fante C, Galasso T, Bernasconi P, et al. Extracorporeal photopheresis as a new supportive therapy for bronchiolitis obliterans syndrome after allogeneic stem cell transplantation. *Bone Marrow Transplant*. 2016;51(5):728-731.

8. Yanik GA, Mineishi S, Levine JE, et al. Soluble tumor necrosis factor receptor: Enbrel (etanercept) for subacute pulmonary dysfunction following allogeneic stem cell transplantation. *Biol Blood Marrow Transplant*. 2012;18(7):1044-1054.

9. Srinivasan M, Flynn R, Price A, et al. Donor B-cell alloantibody deposition and germinal center formation are required for the development of murine chronic GVHD and bronchiolitis obliterans. *Blood*. 2012;119(6):1570-1580.

10. Flynn R, Du J, Veenstra RG, et al. Increased T follicular helper cells and germinal center B cells are required for cGVHD and bronchiolitis obliterans. *Blood*. 2014;123(25):3988-3998.

11. Jonigk D, Rath B, Borchert P, et al. Comparative analysis of morphological and molecular motifs in bronchiolitis obliterans and alveolar fibroelastosis after lung and stem cell transplantation. *J Pathol Clin Res*. 2016;3(1):17-28.

12. von der Thüsen JH, Hansell DM, Tominaga M, et al. Pleuroparenchymal fibroelastosis in patients with pulmonary disease secondary to bone marrow transplantation. *Mod Pathol*. 2011;24(12):1633-1639.

13. Takeuchi Y, Miyagawa-Hayashino A, Chen F, et al. Pleuroparenchymal fibroelastosis and non-specific interstitial pneumonia: frequent pulmonary sequelae of haematopoietic stem cell transplantation. *Histopathology*. 2015;66(4):536-544.

14. Flaherty KT, Robert C, Hersey P, et al; METRIC Study Group. Improved survival with MEK inhibition in BRAF-mutated melanoma. *N Engl J Med*. 2012;367(2):107-114.

15. Ascierto PA, McArthur GA, Dréno B, et al. Cobimetinib combined with vemurafenib in advanced BRAF(V600)-mutant melanoma (coBRIM): updated efficacy results from a randomised, double-blind, phase 3 trial. *Lancet Oncol*. 2016;17(9):1248-1260.

16. Planchard D, Besse B, Groen HJM, et al. Dabrafenib plus trametinib in patients with previously treated BRAF(V600E)-mutant metastatic non-small cell lung cancer: an open-label, multicentre phase 2 trial. *Lancet Oncol*. 2016;17(7):984-993.

17. Kurian N, Cohen TS, Öberg L, et al. Dual role for a MEK inhibitor as a modulator of inflammation and host defense mechanisms with potential therapeutic application in COPD. *Int J Chron Obstruct Pulmon Dis*. 2019;14:2611-2624.

18. Andrikopoulos P, Kieswich J, Pacheco S, et al. The MEK inhibitor trametinib ameliorates kidney fibrosis by suppressing ERK1/2 and mTORC1 signaling. *J Am Soc Nephrol*. 2019;30(1):33-49.

19. Shindo T, Kim TK, Benjamin CL, Wieder ED, Levy RB, Komanduri KV. MEK inhibitors selectively suppress alloreactivity and graft-versus-host disease in a memory stage-dependent manner. *Blood*. 2013;121(23):4617-4626.

20. Itamura H, Shindo T, Tawara I, et al. The MEK inhibitor trametinib separates murine graft-versus-host disease from graft-versus-tumor effects. *JCI Insight*. 2016;1(10):e86331.

21. Itamura H, Shindo T, Yoshioka S, Ishikawa T, Kimura S. Phosphorylated ERK1/2 in CD4 T cells is associated with acute GVHD in allogeneic hematopoietic stem cell transplantation. *Blood Adv*. 2020;4(4):667-671.

22. Nowosad A, Jeannot P, Callot C, et al. p27 controls Ragulator and mTOR activity in amino acid-deprived cells to regulate the autophagy-lysosomal pathway and coordinate cell cycle and cell growth. *Nat Cell Biol*. 2020;22(9):1076-1090.

23. Moelling K, Schad K, Bosse M, Zimmermann S, Schweneker M. Regulation of Raf-Akt cross-talk. *J Biol Chem*. 2002;277(34):31099-31106.

24. Appleman LJ, van Puijenbroek AA, Shu KM, Nadler LM, Boussiotis VA. CD28 costimulation mediates down-regulation of p27kip1 and cell cycle progression by activation of the PI3K/PKB signaling pathway in primary human T cells. *J Immunol*. 2002;168(6):2729-2736.

25. Delgoffe GM, Pollizzi KN, Waickman AT, et al. The kinase mTOR regulates the differentiation of helper T cells through the selective activation of signaling by mTORC1 and mTORC2. *Nat Immunol*. 2011;12(4):295-303.

26. Schetelig J, Chevallier P, van Gelder M, et al. Idelalisib treatment prior to allogeneic stem cell transplantation for patients with chronic lymphocytic leukemia: a report from the EBMT chronic malignancies working party. *Bone Marrow Transplant*. 2021;56(3):605-613.

27. Toda Y, Kono K, Abiru H, et al. Application of tyramide signal amplification system to immunohistochemistry: a potent method to localize antigens that are not detectable by ordinary method. *Pathol Int*. 1999;49(5):479-483.

28. Cooke KR, Kobzik L, Martin TR, et al. An experimental model of idiopathic pneumonia syndrome after bone marrow transplantation: I. The roles of minor H antigens and endotoxin. *Blood*. 1996;88(8):3230-3239.

29. Bonnardel E, Prevel R, Campagnac M, et al. Determination of reliable lung function parameters in intubated mice. *Respir Res*. 2019;20(1):211.

30. Bankhead P, Loughrey MB, Fernández JA, et al. QuPath: open source software for digital pathology image analysis. *Sci Rep*. 2017;7(1):16878.

31. Chan BKC. Data analysis using R programming. *Adv Exp Med Biol*. 2018;1082:47-122.

32. Cheng Y, Tian H. Current development status of MEK inhibitors. *Molecules*. 2017;22(10):E1551.

33. Sarantopoulos S, Ritz J. Aberrant B-cell homeostasis in chronic GVHD. *Blood*. 2015;125(11):1703-1707.

34. Cooke KR, Luznik L, Sarantopoulos S, et al. The biology of chronic graft-versus-host disease: a task force report from the National Institutes of Health Consensus Development Project on Criteria for Clinical Trials in Chronic Graft-versus-Host Disease. *Biol Blood Marrow Transplant*. 2017;23(2):211-234.

35. Leonhardt F, Zirlik K, Buchner M, et al. Spleen tyrosine kinase (Syk) is a potent target for GvHD prevention at different cellular levels. *Leukemia*. 2012;26(7):1617-1629.

36. Poe JC, Jia W, Di Paolo JA, et al. SYK inhibitor entospletinib prevents ocular and skin GVHD in mice. *JCI Insight*. 2018;3(19):122430.

37. Du J, Paz K, Flynn R, et al. Pirfenidone ameliorates murine chronic GVHD through inhibition of macrophage infiltration and TGF-β production. *Blood*. 2017;129(18):2570-2580.

38. Hirota T, Yoshida Y, Kitasato Y, et al. Histological evolution of pleuroparenchymal fibroelastosis. *Histopathology*. 2015;66(4):545-554.

39. Ofek E, Sato M, Saito T, et al. Restrictive allograft syndrome post lung transplantation is characterized by pleuroparenchymal fibroelastosis. *Mod Pathol*. 2013;26(3):350-356.

40. Xu L, Drachenberg C, Tavora F, Burke A. Histologic findings in lung biopsies in patients with suspected graft-versus-host disease. *Hum Pathol*. 2013;44(7):1233-1240.

41. Carmo AA, Costa BR, Vago JP, et al. Plasmin induces in vivo monocyte recruitment through protease-activated receptor-1-, MEK/ERK-, and CCR2-mediated signaling. *J Immunol*. 2014;193(7):3654-3663.

42. Herrero-Sánchez MC, Rodríguez-Serrano C, Almeida J, et al. Targeting of PI3K/AKT/mTOR pathway to inhibit T cell activation and prevent graft-versus-host disease development. *J Hematol Oncol*. 2016;9(1):113.

43. Quan-Jun Y, Yan H, Yong-Long H, et al. Selumetinib attenuates skeletal muscle wasting in murine cachexia model through ERK inhibition and AKT activation. *Mol Cancer Ther*. 2017;16(2):334-343.

44. Ragon BK, Odenike O, Baer MR, et al. Oral MEK 1/2 inhibitor trametinib in combination with AKT inhibitor GSK2141795 in patients with acute myeloid leukemia with RAS mutations: a phase II study. *Clin Lymphoma Myeloma Leuk*. 2019;19(7):431-440.e13.

45. Larkin J, Ascierto PA, Dréno B, et al. Combined vemurafenib and cobimetinib in BRAF-mutated melanoma. *N Engl J Med*. 2014;371(20):1867-1876.

46. Yamaguchi T, Kakefuda R, Tajima N, Sowa Y, Sakai T. Antitumor activities of JTP-74057 (GSK1120212), a novel MEK1/2 inhibitor, on colorectal cancer cell lines in vitro and in vivo. *Int J Oncol*. 2011;39(1):23-31.

47. Itamura H, Shindo T, Muranushi H, et al. Pharmacological MEK inhibition promotes polyclonal T-cell reconstitution and suppresses xenogeneic GVHD. *Cell Immunol*. 2021;367:104410.